RESEARCH ARTICLE

Macromolecular Materials and Engineering
www.mame-journal.de

Dual Post-Treatments Boost Thermoelectric Performance of PEDOT:PSS Films and Their Devices

Ting Wu, Xiao-Lei Shi, Wei-Di Liu, Shuai Sun, Qingfeng Liu, and Zhi-Gang Chen**

Owing to intrinsically high electrical conductivity and low thermoelectric conductivity, poly(3,4-ethylenedioxithiophene):poly(styrenesulfonate) (PEDOT:PSS) shows promising thermoelectric properties. However, its relatively low power factor limits the practical applications of PEDOT:PSS. Here, unique dual post-treatments by sodium sulfite (Na_2SO_3) and formamide (CH_3NO) to boost the thermoelectric performance of flexible PEDOT:PSS films with an optimized power factor of 74.09 μW m^{-1} K^{-2} are used. Comprehensive characterizations confirm that CH_3NO reduces the excessive insulating PSS and thereby increases the electrical conductivity, while Na_2SO_3 lowers the reduction of the doping level of PEDOT, leading to an increased Seebeck coefficient. Furthermore, the rationally post-treated PEDOT:PSS films are assembled into a flexible thermoelectric device that exhibits an open-circuit voltage of 2.8 mV using the heat from the human arm and an output power density of 2.56 μW cm^{-2} by a temperature difference of 25 K, indicating great potential for practical applications on sustainably charging low-grade wearable electronics.

1. Introduction

The ever-growing consumption of fossil fuels leads to serious issues in human society, such as energy depletion and gas/water pollution.[1] Therefore, it is urgent to explore alternative, sustainable, and eco-friendly energy sources. Thermoelectric materials and their related devices can convert waste heat into electrical energy,[2–4] and in turn have gained significant attention in recent decades.[5–8] Their thermoelectric potential can be evaluated by the dimensionless figure-of-merit $ZT = S^2\sigma T/\kappa$, where S, σ, T, and κ are the Seebeck coefficient, electrical conductivity, absolute temperature, and thermal conductivity, respectively.[9,10] The $S^2\sigma$ is described as the power factor for thermoelectric materials. Generally, traditional thermoelectric materials are mostly solid-state inorganics,[11] such as GeTe,[12–14] Cu_2Se,[15] and SnSe[16] that which reported excellent thermoelectric properties with ZTs > 2. However, with the increasing demand for sustainable charging wearable electronics,[17] developing flexible thermoelectric materials and devices[18,19] has become more significant, and exploring new-generation thermoelectric materials with both excellent flexibility and thermoelectric properties is highly needed.

Compared with conventional inorganic thermoelectric materials, organic materials possess unique characteristics such as their high flexibility, low cost, and low toxicity.[6] Till now, many promising conducting polymers, such as polyaniline,[20] polypyrrole,[21,22] poly(3-hexylthiophene),[23,24] and poly(3,4ethylenedioxythiophene):poly(4-styrenesulfonate) (PEDOT:PSS),[8,25–28] have exhibited thermoelectric potential. Among these state-of-the-art conducting polymers, PEDOT:PSS is especially promising because of its highly tunable σ and S. PEDOT:PSS is mainly derived from the polythiophene family. The oxidized state of PEDOT has high σ but is insoluble in the water. Introducing the PSS as the counter-ion to PEDOT allows forming stable PEDOT:PSS water dispersing liquid with a hydrophobic PEDOT-rich core and a hydrophilic PSS-rich outer shell.[29] Generally, pristine PEDOT:PSS possesses poor σ and S, mainly derived from the excessive insulating PSS in the structure and the high oxidation level of PEDOT, respectively.[30] Therefore, extensive researches focus on exploring suitable pre- or post-treatments as well as rational doping or dedoping to tackle these issues and in turn improve the $S^2\sigma$ of PEDOT:PSS,[31–34]

T. Wu, Q. Liu
State Key Laboratory of Materials-Oriented Chemical Engineering
College of Chemical Engineering
Nanjing Tech University
Nanjing 211816, China
E-mail: qfliu@njtech.edu.cn
X.-L. Shi, Z.-G. Chen
School of Chemistry and Physics
Queensland University of Technology
Brisbane, Queensland 4000, Australia
E-mail: zhigang.chen@qut.edu.au
W.-D. Liu
Australian Institute for Bioengineering and Nanotechnology
The University of Queensland
Brisbane, Queensland 4072, Australia
S. Sun
Centre for Future Materials
University of Southern Queensland
Springfield Central, Queensland 4300, Australia

The ORCID identification number(s) for the author(s) of this article can be found under https://doi.org/10.1002/mame.202200411

DOI: 10.1002/mame.202200411

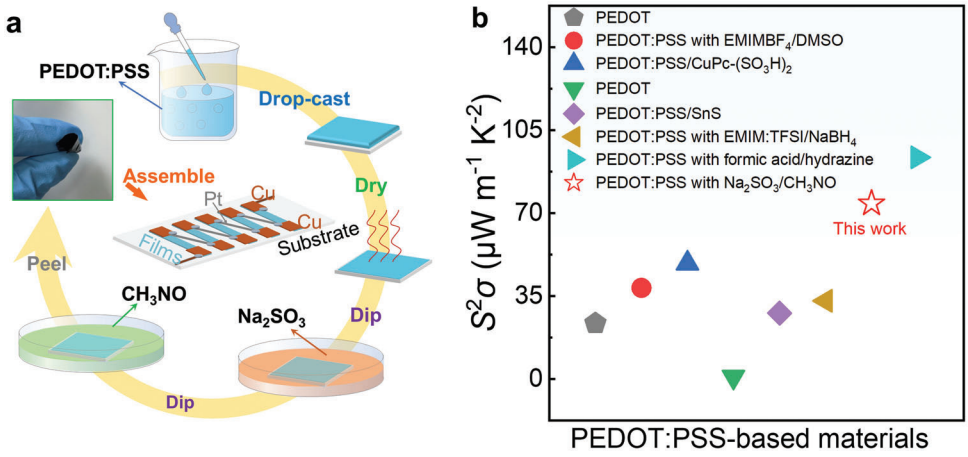

Figure 1. a) Schematic diagram of preparing PEDOT:PSS films post-treated with Na_2SO_3 solution and CH_3NO and thermoelectric devices. The photograph of the as-achieved free-standing PEDOT:PSS film was treated with 90 mmol L^{-1} Na_2SO_3 and CH_3NO. b) Comparison of power factor $S^2\sigma$ between this work and reported PEDOT:PSS-based films.[8,26,32,34–36,38]

while hybridizing with other inorganic/organic materials can trigger effective energy filtering effect to filter the low-energy carriers and in turn improve the S.[8,26] Benefitted from the above effective strategies, up to now, the thermoelectric properties of PEDOT:PSS-based thermoelectric materials have been considerably improved.[8,26,32–37] For example, combining PEDOT:PSS with 8% inorganic SnS was reported to significantly enhance its electrical transport up to 767 S cm^{-1}, leading to an optimized $S^2\sigma$ of 27.8 μW m^{-1} K^{-2}.[26] The copper phthalocyanine disulfonic acid (CuPc–$(SO_3H)_2$)-doped PEDOT:PSS composite films with a high σ of 2.8×10^5 S m^{-1} and a high $S^2\sigma$ of 48.8 μW m^{-1} K^{-2}.[8] Besides, post-treatment by using polar solvents dimethyl sulfoxide (DMSO)[32,33] and acids (H_2SO_4)[37] removes excessive PSS to improve σ while inorganic reducing agents such as sodium borohydride ($NaBH_4$)[34,37] and ionic liquids like 1-ethyl-3methylimidazolium tetrafluoroborate ($EMIMBF_4$)[32] causes dedoping in PEDOT to improve the S. Accordingly, reducers and polar solvents are consequently useful for improving the thermoelectric properties of PEDOT:PSS films.

In this study, high-performing thermoelectric PEDOT:PSS films were prepared by dropping filtered PEDOT:PSS on precleaned glass substrates, then modified with sodium sulfite (Na_2SO_3) and formamide (CH_3NO) dual post-treatments, to improve their thermoelectric properties, as illustrated by **Figure 1**a. The as-achieved free-standing films can be cut into small strips after being separated from the glass substrate. The flexible thermoelectric devices (TEDs) were then fabricated on poly(ethylene terephthalate) (PET) substrates by using the Na_2SO_3–CH_3NO dual-treated films. The as-prepared film exhibits an optimal $S^2\sigma$ of 74.09 μW m^{-1} K^{-2}, which is very competitive compared to those of the reported literature (Figure 1b).[8,26,32,34–36,38] Our comprehensive structural and morphological characterizations suggest that CH_3NO reduces the excessive insulating PSS and thereby increases the σ while the inorganic reducing agent Na_2SO_3 lowers the reduction of the doping level of PEDOT, leading to an increased S. Furthermore, our fabricated TEDs show an open-circuit voltage of 2.8 mV by using the heat from the human arm, indicating that the as-designed high-performing PEDOT:PSS films are promising for applying to wearable TEDs.

2. Results and Discussion

2.1. Thermoelectric Properties of the PEDOT:PSS Films

We firstly investigated the individual effect of CH_3NO and Na_2SO_3 solution on influencing the σ and S of the pristine PEDOT:PSS films. **Figure 2**a shows the measured σ, S, and determined $S^2\sigma$ of the PEDOT:PSS films as the CH_3NO post-treatment time changed. It is clear that the pristine PEDOT:PSS film exhibits a low σ of 0.17 S cm^{-1} and a low S of 15.6 μV K^{-1}. However, the low σ is significantly enhanced from 0.17 to 1058 S cm^{-1} with the post-treatment time prolonged to 30 min. However, the S is not obviously affected by the CH_3NO post-treatment. Figure 2b displays the measured σ, S, and calculated $S^2\sigma$ of the PEDOT:PSS films in relation to the concentration of Na_2SO_3 solution. As can be seen, the S of the films is considerably improved with increasing the Na_2SO_3 concentration. The films treated with 70 mmol L^{-1} Na_2SO_3 exhibits the maximum S of 46 μV K^{-1}. Based on these results, we can conclude that the single treatment by CH_3NO can only effectively improve the σ while the single treatment by Na_2SO_3 solution can only enhance the S. Therefore, in order to further improve the thermoelectric performance of the PEDOT:PSS films, it would be beneficial to develop rational dual post-treatments with CH_3NO and Na_2SO_3.

To explore the optimized treatment time of CH_3NO and concentration of Na_2SO_3 solution during dual post-treatments, we designed crossover experiments. **Figure 3**a–c shows the thermoelectric properties including σ, S, and $S^2\sigma$ of PEDOT:PSS films. These films were first treated with different concentrations of Na_2SO_3 solutions (e.g., 10, 30, 50, 70, 90, and 120 mmol L^{-1}), and then post-treated with CH_3NO at different treatment time. With increasing the CH_3NO treatment time, most samples show increased σ and decreased S. After 90 mmol L^{-1} Na_2SO_3 treatment followed by 30 min CH_3NO treatment, the $S^2\sigma$ of the film is 64 μW m^{-1} K^{-2}, 78% higher than that of the single CH_3NO post-treated film. Figure 3d–f shows the thermoelectric properties including σ, S, and $S^2\sigma$ of PEDOT:PSS films treated with 30 min CH_3NO and Na_2SO_3 solutions with different concentrations in different treatment orders, which include four

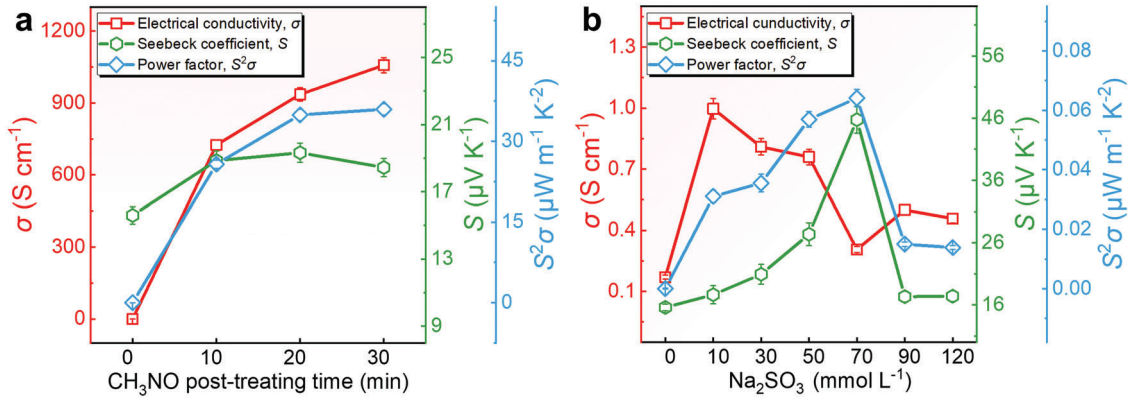

Figure 2. Measured room-temperature electrical conductivity σ, Seebeck coefficient S, and $S^2\sigma$ of PEDOT:PSS films treating with a) CH_3NO as a function of treating time and b) Na_2SO_3 solution in different concentrations.

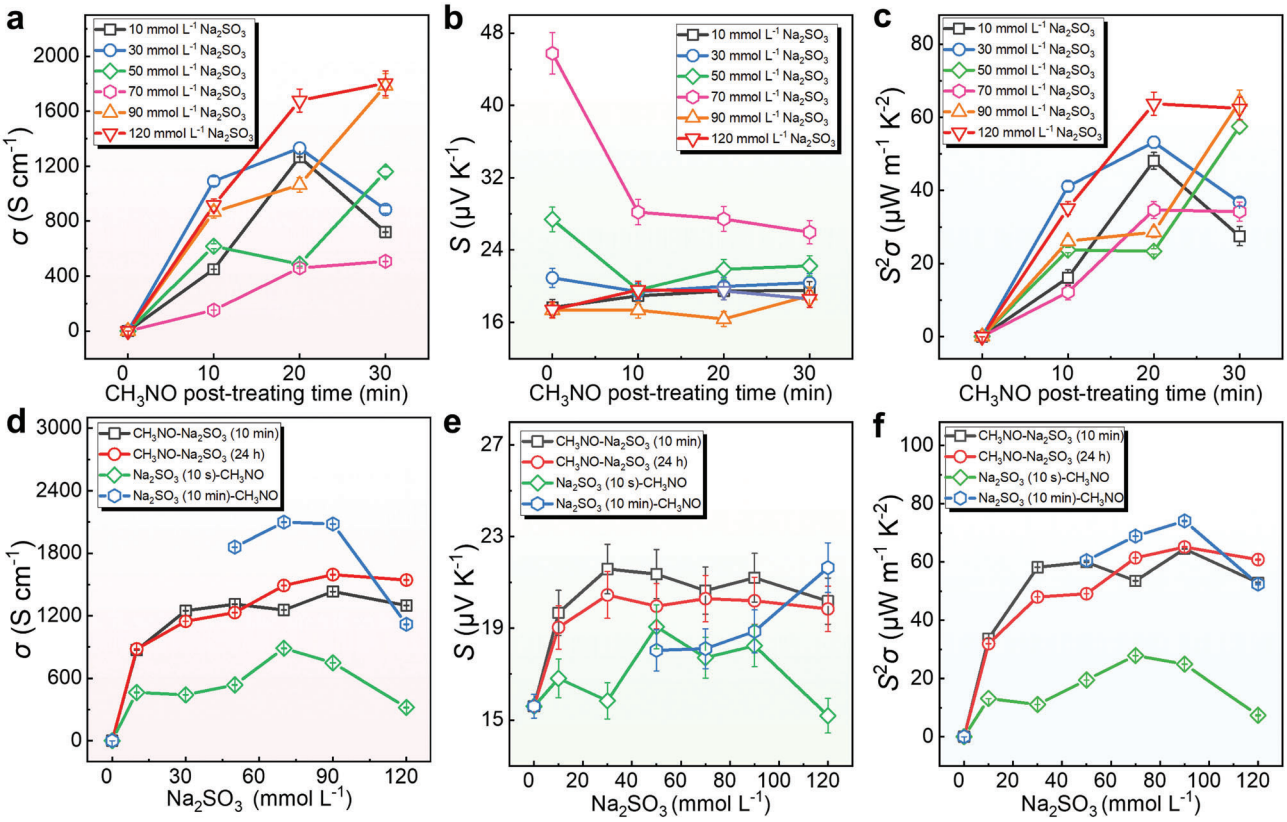

Figure 3. Thermoelectric properties including a) σ, b) S, and c) $S^2\sigma$ of different concentrations of Na_2SO_3-treated PEDOT:PSS films that post-treated with CH_3NO as a function of treatment time. Thermoelectric properties including d) σ, e) S, and f) $S^2\sigma$ of PEDOT:PSS films treated with 30 min CH_3NO and Na_2SO_3 solutions with different concentrations in different treatment orders.

different treating conditions, namely 30 min CH_3NO + 10 min Na_2SO_3 solution, 30 min CH_3NO + 24 h Na_2SO_3 solution, 10 s Na_2SO_3 solution + 30 min CH_3NO, and 10 min Na_2SO_3 solution + 30 min CH_3NO. It should be noted that 10 min (10 and 30 mmol L^{-1}) Na_2SO_3 solutions + CH_3NO treated samples are not observed. Because the films are immersed in low concentrations of Na_2SO_3 solution as shown in Figures S1 and S2 (Supporting Information), the films dissolved, which is derived from the fact that excessive H_2O can dissolve PEDOT:PSS very quickly. We found a significant increase in σ and S after the two-step post-treatments with CH_3NO and Na_2SO_3 solution. The films treated with 70 and 90 mmol L^{-1} Na_2SO_3 solutions for 10 min and then CH_3NO for 30 min both exhibit high σ of more than 2000 S cm^{-1} and appropriate S of around 19 μV K^{-1}, leading to the best $S^2\sigma$ of ≈74 μW m^{-1} K^{-2}. The temperature-dependent thermoelectric properties of the film treated with 10 min 70 mmol L^{-1} Na_2SO_3

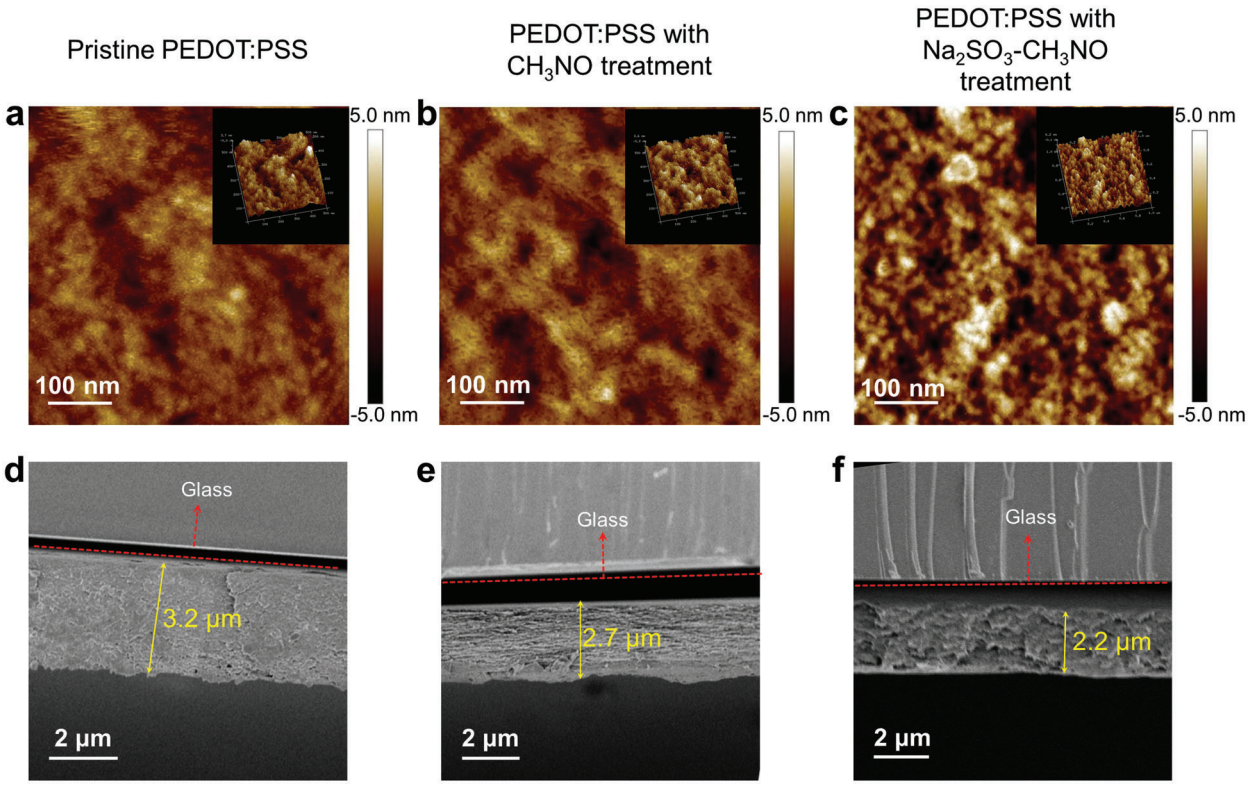

Figure 4. Atomic force microscopy (AFM) images of a) untreated, b) CH_3NO-treated, c) Na_2SO_3–CH_3NO-treated PEDOT:PSS films. The corresponding three-dimensional (3D) AFM images with the same sizes are shown as insets. Scanning electron microscopy (SEM) cross-sectional images of d) untreated, e) CH_3NO-treated, f) Na_2SO_3–CH_3NO-treated PEDOT:PSS films.

and 30 min CH_3NO is shown in Figure S3 (Supporting Information). With increasing the temperature, the σ was decreased from 2018 to 1725 S cm^{-1} and the S was increased from 18 to 24 μV K^{-1}, thus the $S^2\sigma$ was increased from 66 to 99 μW m^{-1} K^{-2}, indicating a typical metallic behavior. Therefore, the charge transport mechanism in PEDOT:PSS films is thermally activated.

2.2. Morphology of the PEDOT:PSS Films

To further understand how dual post-treatments with Na_2SO_3 solution and CH_3NO enhanced thermoelectric properties of PEDOT:PSS films, we performed morphological characterizations on the as-achieved films by scanning electron microscopy (SEM) and atomic force microscopy (AFM). **Figure 4**a–c shows AFM images of the untreated, CH_3NO-treated, Na_2SO_3-CH_3NO-treated PEDOT:PSS films. The CH_3NO post-treated film was treated for 30 min, and the dual-treated film was treated with Na_2SO_3 solution for 10 min followed by CH_3NO for 30 min. The pristine PEDOT:PSS film has a roughness R_q of 1.03 nm in height images, as shown in Figure 4a. Here R_q is the root mean square of the surface roughness. The surface roughness of the CH_3NO-treated PEDOT:PSS film and Na_2SO_3–CH_3NO-treated PEDOT:PSS film is 1.10 and 1.77 nm, respectively, which are slightly higher than the untreated one. Generally, the rough surface is caused by the removal of PSS.[33] PEDOT:PSS is composed of hydrophilic disordered PSS wrapped around ordered PEDOT grains, as indicated by the dark and bright areas on the surface of the pristine films, respectively. After CH_3NO treatment, a distinct "fibrous" structure can be observed in Figure 4b, and a continuous nanofibrous morphology with significant contrast is also witnessed. While after Na_2SO_3–CH_3NO dual treatment, brighter regions are observed on the film surface, as shown in Figure 4c. The as-observed morphology indicates typical phase separation between the conducting PEDOT and the insulating PSS. This is because the hydrophilic CH_3NO resulted in a separation between PEDOT and PSS. The inset corresponding three-dimensional (3D) AFM images in Figure 4a–c exhibit the morphologies of the PEDOT:PSS films under different treatment conditions more directly. Figure 4d–f shows the cross-sectional SEM images of pristine, CH_3NO-treated, and Na_2SO_3-CH_3NO-treated PEDOT:PSS films. The thicknesses of the prepared films were uniform, with the original film thickness of 3.2 μm and the films treated with CH_3NO and Na_2SO_3–CH_3NO dual post-treatments of 2.7 and 2.2 μm, respectively. With the post-treatment of CH_3NO and Na_2SO_3–CH_3NO, the thickness of the film was slightly reduced, which is mainly derived from the removal of PSS.

2.3. Morphology and Structure Characterizations of the PEDOT:PSS Films

To further understand the mechanisms of dual post-treatments on the improved thermoelectric performance of PEDOT:PSS

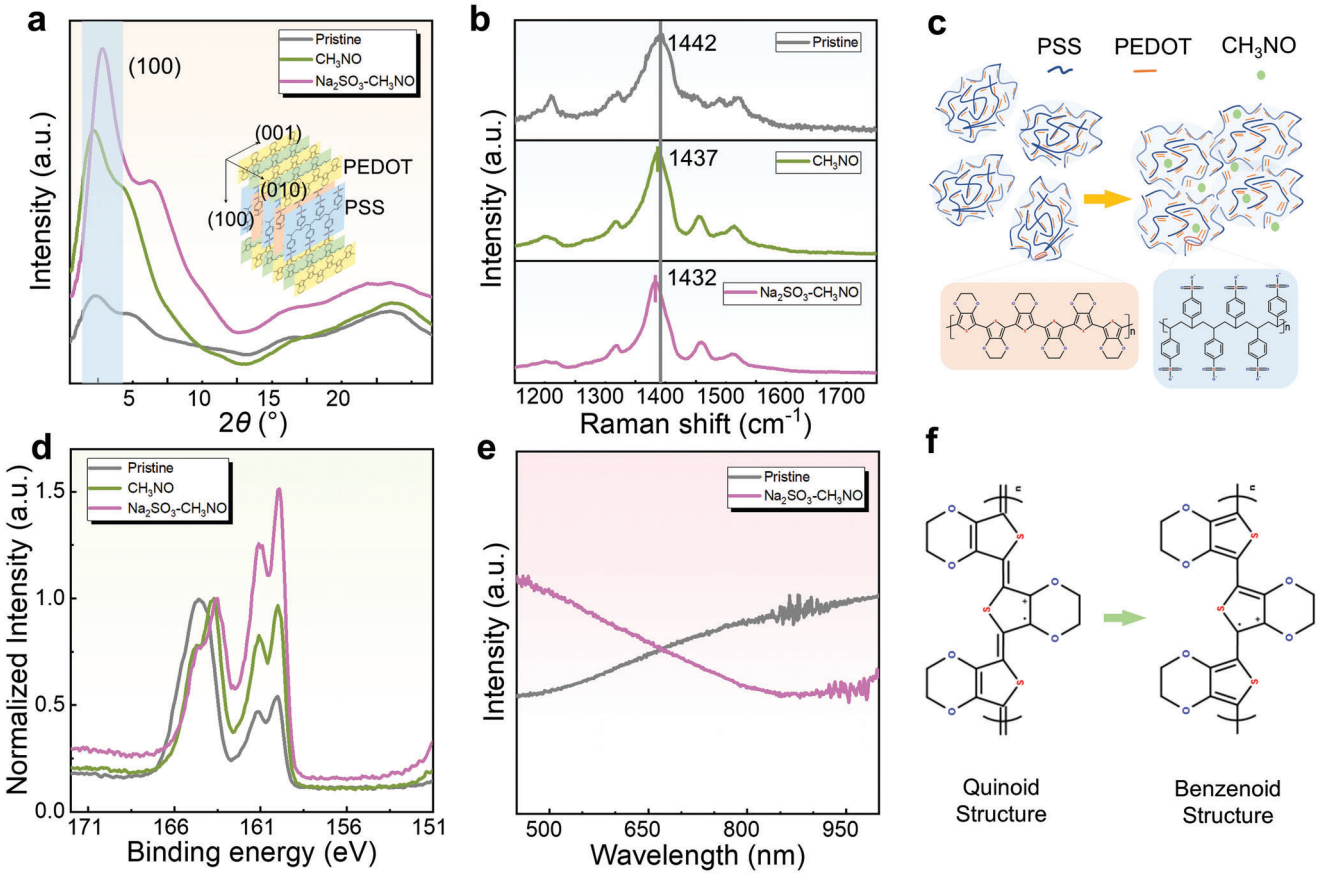

Figure 5. a) X-ray diffraction (XRD) patterns and b) Raman spectra of untreated, CH_3NO-treated, and Na_2SO_3–CH_3NO-treated PEDOT:PSS films. The inset in (a) illustrates the structure of PEDOT:PSS. c) Illustration of structural transformation in CH_3NO-treated PEDOT:PSS. d) X-ray photoelectron spectroscopy (XPS) of pristine, CH_3NO-treated, and Na_2SO_3–CH_3NO-treated PEDOT:PSS films. e) UV–vis absorption spectra of pristine and Na_2SO_3–CH_3NO-treated PEDOT:PSS films. f) Schematic models of the transformation from the quinoid structure to benzenoid structure.

films, we performed X-ray diffraction (XRD), Raman, and UV–vis absorption spectrum characterizations and X-ray photoelectron spectroscopy (XPS). **Figure 5**a,b shows the XRD and Raman spectra of the untreated, CH_3NO-treated, and Na_2SO_3–CH_3NO-treated PEDOT:PSS films. For XRD results, in the pristine film, a characteristic peak is observed at ≈4.7°. The corresponding layers are superimposed on the alternating arrangement of (100) faces of PEDOT and PSS.[39,40] With CH_3NO treatment and Na_2SO_3 treatment, the peaks at ≈4.7° become sharper, indicating an increase in the crystallinity of the films, which is attributed to the effective removal of PSS.[41] This is also in agreement with the AFM results. Figure 5b shows the as-performed Raman spectra of CH_3NO– and Na_2SO_3–CH_3NO-treated PEDOT:PSS. As can be seen, the Raman peak between 1400 and 1500 cm^{-1} is correlated with symmetric $C_\alpha = C_\beta$ stretching.[42,43] For the pristine PEDOT:PSS film, the characteristic peak of PEDOT appears at 1447 cm^{-1}. After CH_3NO treatment, the peak at 1437 cm^{-1} shows a slight shift of 5 cm^{-1}, indicating that the CH_3NO treatment on the change of PEDOT conformation is negligible, confirming that the single CH_3NO treatment has little effect on the *S*. After the two-step treatment with Na_2SO_3 and CH_3NO, the Raman band showed a significant peak shift from 1442 to 1432 cm^{-1}, which is related to the chemical reduction to polariton and neutral states, as well as the degree of deformation of the backbone during the transition between benzoyl and quinone types.[44] The post-treatment with Na_2SO_3 and CH_3NO is accompanied by a shift to lower wavenumbers with a narrowing of the bandwidth, indicating a change in the PEDOT chain from a coiled (benzene ring) to a stretched structure (quinone ring), which favors the σ.[43] The chemical structures of PEDOT and PSS and their structural deductions after CH_3NO treatment are shown in Figure 5c. Formamide is a polar solvent with a high dielectric constant, which can promote the phase separation of PSS from PEDOT. The insulating PSS was taken away by CH_3NO, which promotes the ordered arrangement of the internal conducting PEDOT and reduces the barrier for carrier transport. Figure 5d shows the XPS results of S_{2p} for the PEDOT:PSS films. Generally, the peaks at high binding energy (164.6, 163.7, and 163.4 eV) correspond to the sulfur atoms in the sulfonic acid group in PSS, and the double peaks at low binding energy (160, 160, and 159.9 eV) correspond to the sulfur atoms in the thiophene group in PEDOT.[45] After the CH_3NO–Na_2SO_3 double treatments, the mass ratio of PSS to PEDOT is reduced, indicating that PSS is effectively removed, resulting in the formation of more crystalline PEDOT structures in the film, which is consistent with the XRD pattern. The S_{2p} binding energy of PEDOT at 160 eV is slightly shifted to the low

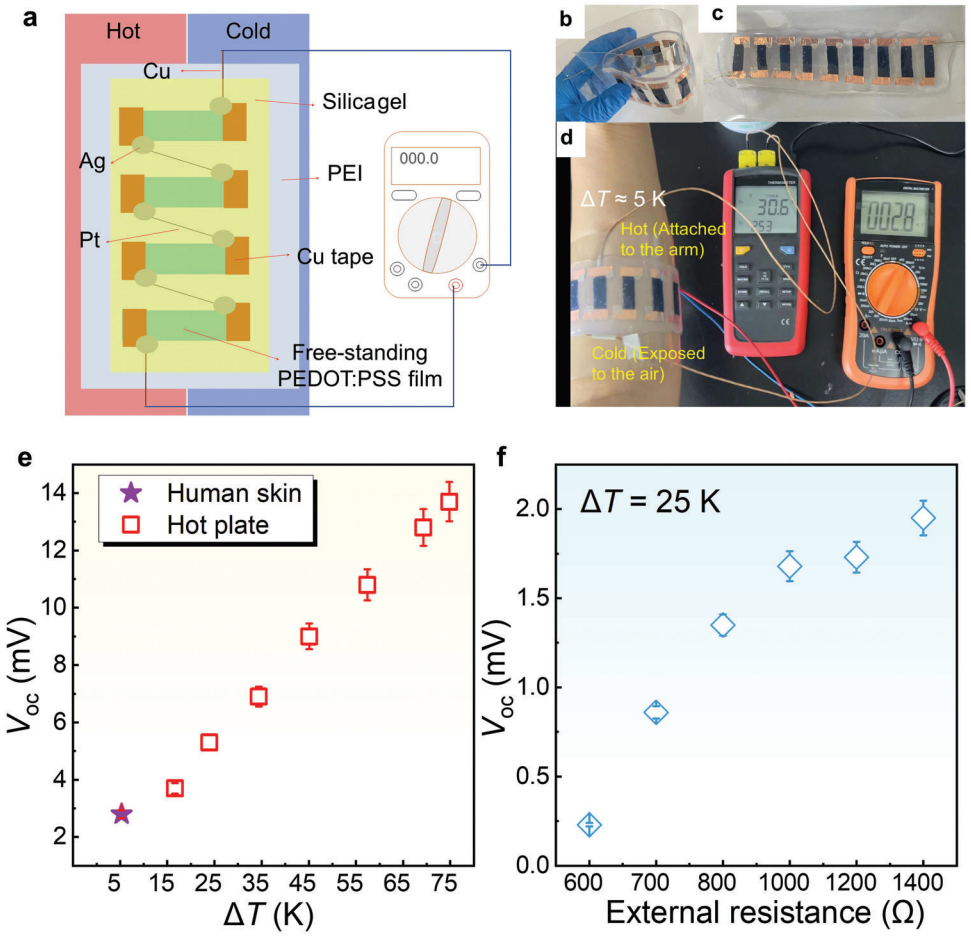

Figure 6. a) Schematic diagram of a thermoelectric device composed of 9-leg of rationally post-treated PEDOT:PSS films as thermoelectric legs connected by platinum wire and output performance test. The substrate is poly(ethylene terephthalate) (PET). Photographs of the packed thermoelectric device b) during bending and c) without bending. d) Photograph to illustrate the open-circuit voltage test by wearing the as-designed device on the human arm as the heat source. e) V_{oc} generated by the device at different temperature difference (ΔTs) using a hot plate and the human skin as heat sources. f) V_{oc} as a function of external resistance.

binding energy (0.1 eV), suggesting that the average oxidation level is reduced by the Na_2SO_3 treatment. The UV–vis absorption spectra of the pristine and Na_2SO_3–CH_3NO-treated PEDOT:PSS films also confirm this phenomenon, as shown in Figure 5e. As can be seen, PEDOT in different oxidation states has significant absorption in different wavelengths. The absorption of neutral monomer and polariton occurs at ≈600 and ≈900 nm.[31] Compared to the untreated PEDOT:PSS, the spectral absorption of the Na_2SO_3–CH_3NO-treated sample increases at 600 nm and decreases at 900 nm, indicating a decrease in the average oxidation level of the sample.[31] After treatment with the reducing agent Na_2SO_3, the dominant state on the PEDOT backbone changes from the polariton state to the neutral state. The absorption band at >900 nm indicates a dipolar-polariton transition of PEDOT chains.[46] After treating with reducing agents, the thiophene ring in PEDOT is transformed from a quinoid structure to benzenoid structure, as shown in Figure 5f. The carrier concentration of PEDOT:PSS is decreased, thus leads to an increased S. After the synergistic effect of the dual treatments with Na_2SO_3 and CH_3NO, PEDOT shows a partial reduction, both σ and S are improved, which is consistent with the change in thermoelectric properties shown in Figure 3.

2.4. Fabrication and Application of the TEDs

To evaluate the application potential of the dual-post-treated films, a prototype of a 9-pair TEDs is designed, and the device structure is provided in **Figure 6**a. The rationally treated PEDOT:PSS films were connected by platinum (Pt) wire, and the substrate is PET. Silver paste and Cuprum (Cu) tape were used at the intersection of films and Pt wire was used to reduce the contact resistance. The identical sizes of all PEDOT:PSS films pieces are 0.7 × 2.5 cm^2. Then silica gel was used to encapsulate the homemade thermoelectric devices to avoid the film from breaking during usage. The as-designed TEDs show good flexibility (Figure 6b,c). When the flexible TEDs were attached to the human arm (Figure 6d), the PET side against the arm acts as the hot side, and the silicone covered side exposed to the air acts as the cold side. The open-circuit voltage V_{oc} is 2.8 mV with a

temperature difference ΔT of 5 K. Figure 6e shows the V_{oc} by the device at different ΔTs using a hot plate and the human skin as heat sources. With increasing the ΔT up to 74 K, a V_{oc} was increased to 14 mV. Figure 6f shows the V_{oc} as a function of load resistance at a ΔT of 25 K.[9] When the load resistance was close to the internal resistance of the device, the maximum output power was 2.8 nW at a ΔT of 25 K. After calculation, the corresponding power density is 2.56 μW cm^{-2}. Our work indicates great application potential for sustainably charging low-grade wearable electronics.

3. Conclusion

To fabricate flexible thermoelectric films with a high power factor, a dual post-treatment with Na_2SO_3 and CH_3NO at room temperature for a PEDOT:PSS film is proposed in this study. The σ of the films is increased from 0.17 to ≈1057.86 S cm^{-1} by CH_3NO treatment under optimized treating time, and the S can be enhanced from 15.6 to 45.76 μV K^{-1} by Na_2SO_3 treatment under optimized concentration. Benefiting from the contributions of both CH_3NO and Na_2SO_3, an optimized power factor of 74.09 μW m^{-1} K^{-2} can be obtained. The polar solvent CH_3NO mainly contributes to the removal of insulating PSS from PEDOT:PSS and yields a highly ordered PEDOT crystal region, which improves the conductivity. The reducing agent Na_2SO_3 can adjust the oxidation and reduction levels of PEDOT and in turn improve the Seebeck coefficient. Besides, TEDs are prepared using rationally treated films, which exhibits an V_{oc} of 2.8 mV when attached to the human arm under indoor conditions. The maximum output power of the TEDs at a ΔT of 25 K is 2.8 nW and the output power density is 2.56 μW cm^{-2}. This work provides inspiration for designing high-performing free-standing PEDOT:PSS films that target sustainably charging low-grade wearable electronics.

4. Experimental Section

Materials and Chemicals: The PEDOT:PSS solution (Clevios PH1000) was purchased from Heraeus. CH_3NO (AR, 99%) was purchased from Aldrich. Ethanol absolute was purchased from Shanghai Lingfeng Chemical Reagent CO., LTD. Acetone was purchased from Shanghai Shenbo Chemical CO., LTD. Na_2SO_3 (AR, 98%) were purchased from Macklin. The syringe filter membrane with a pore size of 0.45 μm was purchased from Tianjin Jinteng Experimental Equipment CO., LTD.

Sample Preparation: The glass substrates (2 × 2 cm) were ultrasonically cleaned with deionized water, acetone and ethanol consecutively then and then cleaned by an ultraviolet ozone machine for half an hour. First, the pristine PEDOT:PSS films were fabricated by filtered PEDOT:PSS solution (200 μL) and then drop-casted onto the pre-cleaned glass substrates. Second, 4 mL of PEDOT:PSS was mixed respectively with 1 mL of (10, 30, 50, 70, 90, 120 mmol L^{-1}) Na_2SO_3 in a beaker and then stirred at 1500 rpm for 24 h, after stirring at 60 °C for 2 h, 200 μL of the Na_2SO_3-treated PEDOT:PSS solutions were filtered with a 0.45 μm syringe filter before drop-casted onto the cleaned glass substrates. Finally, all the samples were dried in a vacuum oven at 60 °C for 2 h and then heated to 90 °C overnight.

CH_3NO Post-Treatment: The pristine PEDT:PSS films were immersed in CH_3NO for 10–30 min and Na_2SO_3-treated PEDOT:PSS films were immersed in CH_3NO for 30 min at room temperature, then rinsed using deionized water to wash away the remnant solvent.

Na_2SO_3/CH_3NO Post-Treatment: The pristine PEDOT:PSS films were soaked in different concentrations (10, 30, 50, 70, 90, and 120 mmol L^{-1}) of Na_2SO_3 for 10 min or 10 s before being immersed in CH_3NO for 30 min as above. The samples were named 10 s Na_2SO_3 solution + 30 min CH_3NO and 10 min Na_2SO_3 solution + 30 min CH_3NO. While in the crossover experiment the pristine PEDOT:PSS films were soaked in different concentrations (10, 30, 50, 70, 90, and 120 mmol L^{-1}) of Na_2SO_3 for 10min or 24 h after being soaked in the CH_3NO for 30 min. The samples were named 30 min CH_3NO + 10 min Na_2SO_3 solution, 30 min CH_3NO + 24 h Na_2SO_3 solution. All the post-treatment samples were cleaned with ethanol or deionized water and dried on a heating table at 120 °C for 10 min.

Thermoelectric Device Fabrication: The 10 min (70 mmol L^{-1}) Na_2SO_3 solution + 30 min CH_3NO films were prepared on 3 × 7.5 cm glass sheets and then soaked in deionized water for a period of time and then peeled away from the glass substrate and obtained free-standing film. The films then were cut into strip shapes with identical sizes of 0.7 × 2.5 cm^2 and assembled on a flexible PET substrate, which was connected in series using the Pt wires to get the thermoelectric generator. Silver paste and Cu tape were used to connect films to Pt wires and the Cu wires were connected at the end of the thermoelectric generator to measure output properties. Finally, the commercially available silicone was spread evenly on the thermoelectric device on PET substrate and dried at room temperature for 48 h. Please note that appropriate ethics committee approval and informed written consent of all participants in this work are obtained (approval number (LP210100020).

Measurement and Characterization: Both the electrical conductivity σ and Seebeck coefficient S of the samples were measured at room temperature with SBA 458 from Netsch. XRD was carried out with D8 Advance from Germany at room temperature using a Cu Kα radiation source. The surface morphology and cross-sectional morphologies of the films were conducted on AFM (Cypher AFM from Asylum Research) and SEM (S-4800). The oxidation levels of the samples were characterized by ultraviolet and visible absorption spectrum (UV–vis absorption spectrum, Lambda 950) and X-ray photoelectron spectroscopy (XPS, Thermo ESCALAB 250, country). Raman spectroscopy was performed from 1200 to 1800 cm^{-1} on a confocal Raman microscope (LabRAM HR Evolution) using a 553 nm laser. The open-circuit voltage of the device was measured using a multimeter and the temperature difference was measured by a thermocouple.

Supporting Information

Supporting Information is available from the Wiley Online Library or from the author.

Acknowledgements

T.W. and X.-L.S. contributed equally to this work. This work was financially supported by the National Natural Science Foundation of China (No. 51972170), the State Key Laboratory of Materials-Oriented Chemical Engineering (No. ZK201812), the Priority Academic Program Development of Jiangsu Higher Education Institutions (PAPD), the Jiangsu Specially appointed Professor Program. Z.G.C. thanks the financial support from the Australian Research Council and the Innovation Centre for Sustainable Steel project.

Open access publishing facilitated by Queensland University of Technology, as part of the Wiley - Queensland University of Technology agreement via the Council of Australian University Librarians.

Conflict of Interest

The authors declare no conflict of interest.

Data Availability Statement

The data that support the findings of this study are available from the corresponding author upon reasonable request.

Keywords

formamide, PEDOT:PSS, post-treatment, sodium sulfite, thermoelectrics

Received: June 20, 2022
Revised: July 6, 2022
Published online: July 27, 2022

[1] L. Zhang, X. L. Shi, Y. L. Yang, Z.-G. Chen, *Mater. Today* **2021**, *46*, 62.
[2] G. H. Kim, L. Shao, K. Zhang, K. P. Pipe, *Nat. Mater.* **2013**, *12*, 719.
[3] Q. Jin, S. Jiang, Y. Zhao, D. Wang, J. Qiu, D.-M. Tang, J. Tan, D.-M. Sun, P.-X. Hou, X.-Q. Chen, K. Tai, N. Gao, C. Liu, H.-M. Cheng, X. Jiang, *Nat. Mater.* **2019**, *18*, 62.
[4] J. He, T. M. Tritt, *Science* **2017**, *357*, 9997.
[5] X.-L. Shi, J. Zou, Z.-G. Chen, *Chem. Rev.* **2020**, *120*, 7399.
[6] S. D. Xu, X. L. Shi, M. Dargusch, C. A. Di, J. Zou, Z. G. Chen, *Prog. Mater. Sci.* **2021**, *121*, 100840.
[7] Q. Jiang, X. Lan, C. Liu, H. Shi, Z. Zhu, F. Zhao, J. Xu, F. Jiang, *Mater. Chem. Front.* **2018**, *2*, 679.
[8] S. Q. Wu, Y. H. Wang, L. Z. Hu, Q. Yin, K. Du, Q. J. Yin, L. B. Huang, *J. Appl. Polym. Sci.* **2021**, *138*, 50883.
[9] S. Sun, X. L. Shi, W. D. Liu, T. Wu, D. Wang, H. Wu, X. Zhang, Y. Wang, Q. Liu, Z. G. Chen, *ACS Appl. Mater. Interfaces* **2022**, *14*, 8066.
[10] L.-C. Yin, W.-D. Liu, X.-L. Shi, H. Gao, M. Li, D.-Z. Wang, H. Wu, L. Kou, H. Guo, Y. Wang, Q. Liu, Z.-G. Chen, *Chem. Eng. J.* **2022**, *433*, 133775.
[11] B. Hu, X.-L. Shi, J. Zou, Z.-G. Chen, *Chem. Eng. J.* **2022**, *437*, 135268.
[12] L. C. Yin, W. D. Liu, M. Li, Q. Sun, H. Gao, D. Z. Wang, H. Wu, Y. F. Wang, X. L. Shi, Q. F. Liu, Z. G. Chen, *Adv. Energy Mater.* **2021**, *11*, 2102913.
[13] D.-Z. Wang, W.-D. Liu, X.-L. Shi, H. Gao, H. Wu, L.-C. Yin, Y. Zhang, Y. Wang, X. Wu, Q. Liu, Z.-G. Chen, *J. Mater. Sci. Technol.* **2022**, *106*, 249.
[14] D.-Z. Wang, W.-D. Liu, M. Li, L.-C. Yin, H. Gao, Q. Sun, H. Wu, Y. Wang, X.-L. Shi, X. Yang, Q. Liu, Z.-G. Chen, *Chem. Eng. J.* **2022**, *441*, 136131.
[15] S. Butt, M. U. Farooq, W. Mahmood, S. Salam, M. Sultan, M. A. Basit, J. Ma, Y. Lin, C.e-W. Nan, *J. Alloys Compd.* **2019**, *786*, 557.
[16] X.-Y. Mao, X.-L. Shi, L.-C. Zhai, W.-D. Liu, Y.-X. Chen, H. Gao, M. Li, D.-Z. Wang, H. Wu, Z.-H. Zheng, Y.-F. Wang, Q. Liu, Z.-G. Chen, *J. Mater. Sci. Technol.* **2022**, *114*, 55.
[17] L. Li, W.-D. Liu, Q. Liu, Z.-G. Chen, *Adv. Funct. Mater.* **2022**, *32*, 2200548.
[18] W.-Y. Chen, X.-L. Shi, J. Zou, Z.-G. Chen, *Small Methods* **2022**, *6*, 2101235.
[19] Z.-G. Chen, W.-D. Liu, *J. Mater. Sci. Technol.* **2022**, *121*, 256.
[20] C. Chungyeon, L. W. Kevin, T. Ping, H. Jui-Hung, Y. Choongho, C. G. Jaime, *Adv. Energy Mater.* **2016**, *6*, 1502168.
[21] L. R. Liang, G. M. Chen, C. Y. Guo, *Mater. Chem. Front.* **2017**, *1*, 380.
[22] S. Liu, H. Li, X. Fan, C. He, *Compos. Sci. Technol.* **2022**, *221*, 109347.
[23] M. He, J. Ge, Z. Lin, X. Feng, X. Wang, H. Lu, Y. Yang, F. Qiu, *Energy Environ. Sci.* **2012**, *5*, 8351.
[24] A. M. Glaudell, J. E. Cochran, S. N. Patel, M. L. Chabinyc, *Adv. Energy Mater.* **2015**, *5*, 1401072.
[25] S. D. Xu, M. Hong, X. L. Shi, M. Li, Q. Sun, Q. X. Chen, M. Dargusch, J. Zou, Z. G. Chen, *Energy Environ. Sci.* **2020**, *13*, 3480.
[26] X. J. Cheng, L. Wang, X. Wang, G. M. Chen, *Compos. Sci. Technol.* **2018**, *155*, 247.
[27] L. Zhang, B. Xia, X.-L. Shi, W.-D. Liu, Y. Yang, X. Hou, X. Ye, G. Suo, Z.-G. Chen, *Carbon* **2022**, *196*, 718.
[28] X. Liu, X.-L. Shi, L. Zhang, W.-D. Liu, Y. Yang, Z.-G. Chen, *J. Mater. Sci. Technol.* **2023**, *132*, 81.
[29] J. Rivnay, S. Inal, B. A. Collins, M. Sessolo, E. Stavrinidou, X. Strakosas, C. Tassone, D. M. Delongchamp, G. G. Malliaras, *Nat. Commun.* **2016**, *7*, 11287.
[30] T. Stöcker, A. Köhler, R. Moos, *J. Polym. Sci., Part B: Polym. Phys.* **2012**, *50*, 976.
[31] N. Saxena, J. Keilhofer, A. K. Maurya, G. Fortunato, J. Overbeck, P. Muller-Buschbaum, *ACS Appl. Energy Mater.* **2018**, *1*, 336.
[32] J. Luo, D. Billep, T. Waechtler, T. Otto, M. Toader, O. Gordan, E. Sheremet, J. Martin, M. Hietschold, D. R. T. Zahnd, T. Gessner, *J. Mater. Chem. A* **2013**, *1*, 7576.
[33] Y. Xu, Z. Liu, X. Wei, J. Wu, J. Guo, B. Zhao, H. Wang, S. Chen, Y. Dou, *Synth. Met.* **2021**, *271*, 116628.
[34] J. Atoyo, M. R. Burton, J. McGettrick, M. J. Carnie, *Polymers* **2020**, *12*, 559.
[35] O. Bubnova, M. Berggren, X. Crispin, *J. Am. Chem. Soc.* **2012**, *134*, 16456.
[36] J. Zhao, D. X. Tan, G. M. Chen, *J. Mater. Chem. C* **2017**, *5*, 47.
[37] S. D. Xu, M. Hong, X. L. Shi, Y. Wang, L. Ge, Y. Bai, L. Z. Wang, M. Dargusch, J. Zou, Z. G. Chen, *Chem. Mater.* **2019**, *31*, 5238.
[38] T. A. Yemata, Y. Zheng, A. K. K. Kyaw, X. Z. Wang, J. Song, W. S. Chin, J. W. Xu, *RSC Adv.* **2020**, *10*, 1786.
[39] K. E. Aasmundtveit, E. J. Samuelsen, L. A. A. Pettersson, O. Inganas, T. Johansson, R. Feidenhans, *Synth. Met.* **1999**, *101*, 561.
[40] N. Kim, B. H. Lee, D. Choi, G. Kim, H. Kim, J. R. Kim, J. Lee, Y. H. Kahng, K. Lee, *Phys. Rev. Lett.* **2012**, *109*, 106405.
[41] X. Z. Wang, A. K. K. Kyaw, C. L. Yin, F. Wang, Q. Zhu, T. Tang, P. I. Yee, J. W. Xu, *RSC Adv.* **2018**, *8*, 18334.
[42] A. K.o K.o Kyaw, T. A. Yemata, X. Wang, S. L. Lim, W. S. Chin, K. Hippalgaonkar, J. Xu, *Macromol. Mater. Eng.* **2018**, *303*, 1700429.
[43] J. Ouyang, Q. Xu, C.-W. Chu, Y. Yang, G. Li, J. Shinar, *Polymer* **2004**, *45*, 8443.
[44] J. Luo, D. Billep, T. Blaudeck, E. Sheremet, R. D. Rodriguez, D. R. T. Zahn, M. Toader, M. Hietschold, T. Otto, T. Gessner, *J. Appl. Phys.* **2014**, *115*, 054908.
[45] X. Crispin, F. L. E. Jakobsson, A. Crispin, P. C. M. Grim, P. Andersson, A. Volodin, C. Van Haesendonck, M. Van Der Auweraer, W. R. Salaneck, M. Berggren, *Chem. Mater.* **2006**, *18*, 4354.
[46] Y. Wang, C. Zhu, R. Pfattner, H. Yan, L. Jin, S. Chen, F. Molina-Lopez, F. Lissel, J. Liu, I. Rabiah Noelle, Z. Chen, W. Chung Jong, C. Linder, F. Toney Michael, B. Murmann, Z. Bao, *Sci. Adv. 3*, e1602076.

